

DELIVERABLES

Appendix 1: Research Report

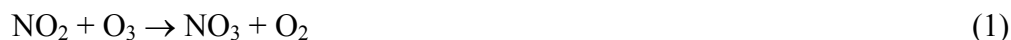
Nitryl Chloride Measurements in the Lower Fraser Valley Airshed

Introduction

It is well-recognized that the Lower Fraser Valley (LFV) is prone to episodes of poor air quality, in part because of its geography, which facilitates stagnation periods and trapping of airborne pollutants near the surface, and also because of continued growth of population and associated emissions from urban, suburban, agricultural and marine sources. Of special concern have been repeated exceedences of the Canada Wide Standard at Hope, located in the eastern part of the LFV. These exceedences have occurred in spite of ongoing declines in emission factors of both nitrogen oxides (NO_x) and volatile organic compounds (VOCs) resulting from the introduction of new vehicle standards and local vehicle testing programs. The lack of a decline in O₃ over the past 15 years coupled with more recent O₃ exceedences, triggering air quality advisories, have made O₃ management in the LFV a priority at all levels of government.

Previous large-scale studies in the LFV, such as Pacific 1993 [*Steyn et al.*, 1997] and Pacific 2001 [*Vingarzan and Li*, 2006] have added important information regarding atmospheric processes leading to O₃ formation. The transformation of primary (e.g., NO_x, VOCs, SO_x, NH₃, etc.) to secondary pollutants (e.g., O₃, fine particulate matter) is highly complex, and the scientific understanding of these highly non-linear processes remains incomplete. *Ainslie and Steyn* (2007) have investigated 20 years of O₃ air quality data in the LFV region and concluded that buildup of a "mystery precursor", prior to the exceedence day, plays an important role in the spatial pattern on exceedence days.

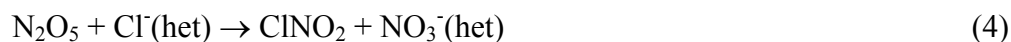
There is now considerable evidence (from modeling studies [*Knipping and Dabdub*, 2003], laboratory investigations [*Raff et al.*, 2009], and field studies [*Osthoff et al.*, 2008; *Tanaka et al.*, 2003]) that "active chlorine" released from sea salt can negatively affect air quality in coastal regions. One pathway to activate chlorine from sea salt is heterogeneous uptake of N₂O₅ on chloride containing aerosol at night. N₂O₅ is formed from the reversible reaction of NO₂ with the nitrate radical (NO₃), which in turn is formed from reaction of NO₂ with O₃.



Heterogeneous hydrolysis of N₂O₅ has long been recognized as an important nocturnal NO_x and O₃ removal pathway.



Uptake of N_2O_5 on chloride containing aerosol yields nitryl chloride (ClNO_2) [Behnke et al., 1997; Finlayson-Pitts et al., 1989]:



Formation of ClNO_2 impacts air quality in the following ways: Since ClNO_2 is formed at night and generally non-reactive, its primary fate is photo-dissociation (to Cl and NO_2) in the early morning hours after sunrise. The photolysis process regenerates NO_2 , which goes on to catalyze O_3 production. The Cl atom is highly reactive towards hydrocarbons and will initiate radical chemistry that produces O_3 and, eventually, secondary aerosol [Behnke et al., 1997]. The fate and impact of ClNO_2 is thus similar to that of nitrous acid (HONO), which also accumulates during the night and photodissociates in the morning to release NO and OH , that go on to produce O_3 (e.g., [Alicke et al., 2003]).

Recently, Osthoff and co-workers [2008] discovered that the rate and impact of the nocturnal heterogeneous conversion of N_2O_5 to ClNO_2 (reaction 4), which also converts unprocessed sea salt to processed sea salt aerosol, has been considerably underestimated. Data collected during the Texaqs 2006 campaign have shown that reaction (4) proceeds efficiently even on primarily non-sea salt surfaces. In the nocturnal polluted marine boundary layer, up to 15% of NO_y has been observed to transform to ClNO_2 [Osthoff et al., 2008]. The efficiency of reaction (4) on aerosol of medium-to-low chloride content has recently been confirmed by several laboratory investigations [Bertram and Thornton, 2009; Raff et al., 2009; Roberts et al., 2009]. Some ambiguity remains as to the detailed mechanism of the reaction, but there is agreement that acid displacement of HCl from supermicron (predominantly sea salt aerosol) to submicron (predominantly non-sea salt aerosol) is a key step in the efficient production of ClNO_2 . These results thus provide strong evidence that this chemistry is active anywhere where pollution and marine air come in contact. However, while the yield of ClNO_2 in reaction (4) is high, the ClNO_2 yield relative to the amount of NO_3 produced from reaction (1) cannot be easily predicted because NO_3 is consumed by other reactions, e.g., with biogenic VOCs such as α -pinene:



Previous studies in the LFV [McLaren et al., 2004] have shown active occasional episodes of active nocturnal N_2O_5 chemistry and have indicated unexplained deficits of up to 9% in the nocturnal NO_y budget [Hayden et al., 2004]. Efficient formation of ClNO_2 is a plausible explanation for this deficit and would be consistent with the "mystery ozone precursor" proposed by Ainslie and Steyn. Thus, the impact of ClNO_2 in the LFV may be large yet but is currently unconstrained by observations.

Furthermore, ClNO_2 is known to convert to Cl_2 on acidified aerosol [Roberts et al., 2008]. In the Eastern LFV, accumulation mode aerosol are likely to be fully neutralized [Anlauf et al., 2006]; the heterogeneous chemistry of ClNO_2 on such aerosol is currently poorly constrained by laboratory studies and field measurements.

Here, a two week data set of co-located measurements of N_2O_5 , ClNO_2 and Cl_2 and other relevant species at T45 in the LFV are presented. These data will allow a first determination of the relative importance of Cl containing radical reservoir species to constrain the extent of their chemistry and impact on regional air quality in the LFV.

Objectives

The objectives of this pilot study were to answer the following questions:

1: NO_y budgets. What are the abundances of ClNO_2 and Cl_2 in the LFV at night when the region is prone to episodes of poor air quality? Specifically, what are the yields of ClNO_2 with respect to the nocturnal production rate of NO_3 ? How are these yields affected by the emission of monoterpenes and isoprene from vegetation? What is the impact of ClNO_2 formation on the effective lifetime of NO_x and on the odd nitrogen (NO_y) budget in the region?

2: Radical sources and O_3 formation. To what extent does the nocturnal conversion of NO_x to ClNO_2 and Cl_2 add to the production of radicals and, ultimately, O_3 in the LFV?

Experimental

A pilot study was conducted during the period of July 20 – August 4, 2012 and focused on the characterization of nocturnal radical and NO_x reservoirs (N_2O_5 and ClNO_2) and daytime photochemistry in the LFV atmosphere. The measurements were conducted at the routine monitoring site near the Abbotsford airport (T45). A side objective was to evaluate the site's suitability for future measurements and, if so, establish a baseline for future measurements. An overview of the measurements conducted by the University of Calgary and partners are given in Tables 1 through 3, respectively. Measurement method, highest time resolution, uncertainty, and current status of the data are indicated (when known).

Results and analysis

Major nitrogen oxides

Figure 1 gives an overview of the major nitrogen oxides observed during this study. Median observed mixing ratios were: $\text{NO}_y = 6.0$ parts-per-billion by volume (ppbv), $\text{NO}_2 = 5.9$ ppbv, and $\text{NO} = 0.9$ ppbv. These concentration levels are typical of an urban air mass impacted by fresh emissions (such as from combustion engines in automobiles).

Figure 2 shows the time-of-day-dependence of NO , NO_2 , and $\text{NO}_x (= \text{NO} + \text{NO}_2)$. The latter is a useful quantity to reduce the effects of daytime photochemistry, i.e., the oxidation of NO by O_3 to form NO_2 which is opposed by NO_2 photolysis:



Mixing ratios of NO and NO_x were highest in the morning hours. Concentration changes at this time of day are difficult to interpret since the nocturnal boundary layer breaks up during this time, resulting in (vertical) mixing of air masses. Further, photolabile species (e.g., ClNO_2 , HONO , N_2O_5 , etc.) that accumulated overnight begin to photodissociate, and local emissions change with the onset of rush hour. In contrast, an afternoon/early evening maximum in NO was absent. This can be rationalized by a greater abundance of oxidants that oxidize NO to NO_2 , i.e., O_3 (see Figures 3 and 4) and organic peroxy radicals, in the afternoon than in the morning hours.

At night, emissions of NO were at a minimum, and NO was oxidized (to NO_2 and higher nitrogen oxides) by O_3 via reaction (6). Accordingly, mixing ratios of NO_2 were highest at night, which was amplified further by lower nocturnal mixing heights.

Mixing ratios of NO_x were lowest in the middle of day and highest at night to the early morning. The day-night trend observed for NO_x can be rationalized from the expected time-of-day dependence of mixing height at this site, which was highest during the day (greatest mixing volume and dilution and hence lowest concentration) and lowest at night (shallow mixing volume, and hence less dilution and higher concentrations). Furthermore, the daytime sink for NO_x (i.e., reaction of NO_2 with OH) is largest in the middle of the day.

Ozone and odd oxygen

Figure 3 shows the time series of ozone and odd oxygen ($\text{O}_x = \text{O}_3 + \text{NO}_2$) for the entire campaign. In general, O_3 mixing ratios were lower than their seasonal average

during this campaign, with maximum value of 66 ppbv on Aug. 4. This was partly a result of lower than average temperatures.

Figure 4 shows the time-of-day dependence (median and 25% and 75% percentiles) of O_3 and O_x ($= O_3 + NO_2$). The latter is a useful quantity in regions with primary emissions of NO (such as this study area), which titrate O_3 to NO_2 . Figure 4 shows that the mixing ratios of O_3 exhibit a clear diurnal profile, with clear daytime photochemical production. The nocturnal titration of O_3 is quite pronounced, often approaching zero ppbv of residual O_3 (e.g., nights of July 25/26, July 26/27, and Aug 2/3, 3/4). The observed nocturnal titration cannot be rationalized by reaction (6) alone, as then O_x should have been conserved, which it is clearly not (Figure 4). Thus, there was considerable and fast dry deposition of O_3 at night. A plausible explanation is that the nearby raspberry fields, which are a primary source of unsaturated hydrocarbons [Malowicki *et al.*, 2008], contributed to the fast nocturnal depletion of O_3 . Furthermore, it is likely that the nocturnal boundary layer at this site was fairly shallow (possibly only several 10s of m).

Nocturnal nitrogen oxides (N_2O_5 and $ClNO_2$) and Cl_2

Figure 5 shows the observed mixing ratios of the nocturnal nitrogen oxides N_2O_5 and $ClNO_2$ for the entire campaign. One of the consequences of the low nocturnal O_3 mixing ratios at this site was that the local NO_3 (and hence N_2O_5 and $ClNO_2$) production rates were modest (average 124 pptv hr^{-1} , median 96 pptv hr^{-1}). Mixing ratios of N_2O_5 reached a maximum of 32 parts-per-trillion by volume (pptv) and were often below detectable limits. Since N_2O_5 is measured by cavity ring-down spectroscopy (in which inverse ring-down time constants, $1/\tau$, are subtracted from inverse blank ring-down time constants, $1/\tau_0$), the observed values scatter around zero (and include negative values) for data below the detection limit.

The $ClNO_2$ mixing ratios were quite small and much lower than reported anywhere else to date, including in the Gulf of Mexico [Osthoff *et al.*, 2008], New England [Kercher *et al.*, 2009], California [Riedel *et al.*, 2012], Calgary [Mielke *et al.*, 2011], or central Europe [Phillips *et al.*, 2012]. There was no indication for the presence of Cl_2 . The low $ClNO_2$ levels observed in this study are rationalized by the low NO_3 production rate (due to low O_3 mixing ratios), likely also by the high sinks for NO_3 (which, just as O_3 , is fairly reactive towards unsaturated hydrocarbons), and N_2O_5 hydrolysis, which directly competes with $ClNO_2$ formation. The equilibrium ratio of $N_2O_5:NO_3$, which determines whether reactions of N_2O_5 or those of NO_3 dominate the nocturnal chemistry, was 24:1 on average. On the night with the largest $ClNO_2$ mixing ratio (Aug 3), it was 60:1. More insight these processes will be possible once the study partners at Environment Canada release their data.

In addition, $ClNO_2$ exhibited a highly unusual diurnal profile, with its maximum mixing ratio observed approximately 1.5 hours after sunrise (Figure 6). This can be explained by $ClNO_2$ formation in a layer above (and decoupled from) the surface

boundary layer followed by subsequent vertical mixing after sunrise. The ClNO₂ morning peak was a persistent feature of this data set (Figure 5).

Figure 7 shows a close-up of the night when the highest N₂O₅ and ClNO₂ mixing ratios (27 and 116 pptv, respectively) were observed. These levels constituted up to 1.6% and 2.6% of NO_y. At the beginning of the night, there was more N₂O₅ than ClNO₂, whereas at the end of the night, there was much more ClNO₂ than N₂O₅. This is expected as the N₂O₅ intermediate converts into the more stable ClNO₂, which accumulates. This particular night was characterized by unusual meteorology: There was an unusually firm nocturnal wind from the SW to W at 8 km/hr. On most other nights, on the other hand, winds were lighter and from more variable directions (typically from the East). Local wind speeds and direction can be deceptive, though. Figure 8 shows Hysplit back-trajectories (~18 hours, injection height 10 m above ground) which clearly connects the measurement site with air that was in contact with ocean water.

Figure 9 shows a comparison of observed ClNO₂ mixing ratios with the output of a simple photochemical box model (kinetic parameters were from the NASA-JPL recommendation [Sander *et al.*, 2006]). In this model, the aerosol surface area density S(aerosol) was set to a constant value of 200 μm² cm⁻³ (to be updated once SMPS data become available), the N₂O₅ (reactive) uptake probability (reaction 3), γ(N₂O₅), was set to a constant value of 0.025, and the branching ratio between reactions 4 and 3, also known as the "ClNO₂ yield", φ(ClNO₂), was set to 10%. Loss of NO₃ to hydrocarbons was not included in this model simulation.

The box model generally overestimates the observed ClNO₂ mixing ratios, except for periods after sunrise (believed to be affected by vertical mixing) and the night of August 1/2 (shown in Figure 10, compared to a slightly altered model with higher ClNO₂ yield). Plausible explanations are the presence of reactions of NO₃ with hydrocarbons (likely) or lower ClNO₂ yields at this site.

It also appears that ClNO₂ was removed faster in the morning than can be rationalized by ClNO₂ photolysis alone. The reason for this could be transport of air containing ClNO₂ out of the study region, or chemistry (i.e., chemical loss of ClNO₂).

There are several plausible explanations for the low yields and faster than expected loss of ClNO₂ in the mornings, that will be subject of future studies: (1) The low ClNO₂ yields are mainly due to the competing reactions of NO₃ with unsaturated hydrocarbons (e.g., reaction (5)). VOCs were quantified during this campaign (by Environment Canada). Unfortunately, the VOC data were not available at the time of this report to test this hypothesis. (2) It is also plausible that there was an insufficient amount of aerosol chloride at this location. Aerosol composition was measured during this campaign (by Environment Canada), but the data were not yet available at the time of this report. (3) There is a currently unknown ClNO₂ loss mechanism. One possible pathway is ClNO₂ loss on partially to fully neutralized aerosol (high levels of NH₃ were encountered during this study). However, this hypothesis would need to be validated by a

laboratory ClNO₂ uptake study. (4) The observed trends are due to transport and hence are not properly described by a simple box model.

PAN and PPN

Peroxy-carboxylic nitric anhydrides (PANs, general structure RC(O)O₂NO₂) are important NO_x reservoir species and are produced as by-products during photochemical ozone production and biomass burning [Roberts, 2007]. Figure 11 shows PAN (CH₃C(O)O₂NO₂) and PPN (C₂H₅C(O)O₂NO₂) data collected during the campaign. Mixing ratios of PAN ranged from ~8 pptv to just under 2 ppbv. PPN ranged from its detection limit of ~20 pptv to ~200 pptv and was below its detection limits on many days.

PAN exhibited a strong diurnal profile (Figure 12), which strongly correlated with that of O₃. This is consistent with a short PAN lifetime (with respect to its thermal decomposition) such that the concentration of PAN scaled with the PAN production rate. Figure 13 shows scatter plots of PAN and PPN against O₃, confirming their relationship.

Figure 14 shows a time series of the ratio of PAN to NO_y. A prior study in the LFV showed PAN:NO_y values of 5% on average [Hayden *et al.*, 2004]. The PAN:NO_y ratio in this campaign was on average 3.3% (median value: 1.5%) and ranged from 0.06% (on the rainy night of July 21/22) to 42% on August 4.

Ratios of PAN species are good indicators of VOCs that contribute to the VOC-NO_x photochemistry. For example, PPN to PAN ratios of 15 - 20% are indicative of anthropogenic hydrocarbon dominated O₃ production, whereas lower PPN: PAN ratios are indicative of biogenic hydrocarbon dominated O₃ production [Grosjean *et al.*, 1996; Roberts *et al.*, 2002; Roberts *et al.*, 1998]. Figure 15 shows a scatter plot of PPN to PAN for the entire campaign. For the subset of data collected on Aug 3, the slope was 0.156, whereas the slope of the data on Aug 4 was 0.103. This indicates that anthropogenic hydrocarbons (such as propene) contributed more to O₃ formation on Aug 3 than they did on Aug 4. A likely factor contributing to this shift in chemical regime was the temperature, which was higher on Aug 4 (max. 31 °C) than on Aug 3 (max. 28 °C); evaporation of VOCs from vegetation increases exponentially with temperature [Koppmann, 2007].

Photolysis frequencies

During daytime, UV radiation is one of the key parameters controlling tropospheric chemistry, including photochemical ozone production and ClNO₂ photodissociation. To understand and model these processes, it is essential to have knowledge of photolysis rates (also called frequencies), which are defined as the first-order loss rate coefficients (*j*, in units of s⁻¹) for each photolysis species. In this study, photolysis frequencies were measured by spectral radiometry [Hofzumahaus *et al.*, 2002;

Hofzumahaus et al., 1999; *Junkermann et al.*, 2002; *Kraus and Hofzumahaus*, 1998; *Stark et al.*, 2007].

Figure 17 shows photolysis frequencies collected during the campaign. For the calculation of $j(\text{ClNO}_2)$, the updated cross-sections reported by *Ghosh et al.* [2011] were used. These data were used to constrain simple photochemical box models of ClNO_2 abundances, to investigate the daytime photostationary state that exists between NO and NO_2 , and to estimate photochemical O_3 production rates.

Figure 18 shows a comparison of measured photolysis frequencies with values predicted using NCAR's TUV model (<http://cprm.acd.ucar.edu/Models/TUV/>) version 4.1 and a surface albedo of 15%. Since the TUV model does not include clouds, a by-and-large cloud-free day (Aug 3) was selected for this comparison. The data are in excellent agreement. This suggests that future studies in the area can utilize the NCAR model without loss of accuracy, at least on cloud-free days.

O_3 production and loss rates

Reactions (6-7) are sufficiently fast such that a so-called photostationary state (pss) is usually established between oxidation of NO by O_3 and photodecomposition of NO_2 during daytime [*Leighton*, 1961].

$$[\text{NO}_2] : [\text{NO}] = k_7[\text{O}_3]/j(\text{NO}_2) \quad (8)$$

In regions with significant O_3 production, the pss is "perturbed" (i.e., shifted towards NO_2) because organic peroxy radicals oxidize NO to NO_2 . The instantaneous production rate of O_3 , $P(\text{O}_3)$, can then be estimated from this perturbation using the following expression [*Thornton et al.*, 2002]:

$$P(\text{O}_3) = j(\text{NO}_2)[\text{NO}_2] - k_7[\text{NO}][\text{O}_3] \quad (9)$$

Figure 19 shows $P(\text{O}_3)$ calculated for the entire campaign (filtered for $j(\text{NO}_2) > 1 \times 10^{-4} \text{ s}^{-1}$, i.e., daytime). There is a lot of scatter in the data; such deviations from the pss occur when measurements are close to sources, such as fresh automobile emissions. Nevertheless, the daily trends are quite clear. The instantaneous O_3 production rate was highly variable between days and ranged from 4 pptv/s on July 23 to above 40 pptv/s on July 26 and Aug 3 and 4. On July 23, the O_3 mixing ratio peaked around 18 ppbv (which is well below the continental average), whereas July 23, Aug 3 and 4 were the days with the highest O_3 concentrations observed during the study (Figure 3). An O_3 production rate in excess of 40 pptv s^{-1} (150 ppbv hr^{-1}) is *very* large. To put this value in context, *Thornton et al.* reported $P(\text{O}_3)$ values of between 5 and 10 pptv s^{-1} during episodes of high O_3 production in Nashville, TN, a region which regularly experiences high oxidant levels [2002].

Figure 20 shows $P(O_3)$ plotted as a function of time of day and color-coded by air temperature. The largest $P(O_3)$ values were observed mid-day and at air temperatures >25 °C. This is consistent with hydrocarbon-limited O_3 production, as biogenic hydrocarbon emissions scale with temperature.

In spite of the very large $P(O_3)$, the net production of O_3 (and O_x) was only modest. Figure 21 shows a time series of $d[O_3]/dt$, averaged over 30 min to reduce the scatter, and Figure 22 shows the time-of-day dependence. The median net O_3 production was 0.6 pptv s^{-1} ($2.2 \text{ ppbv } O_3 \text{ hr}^{-1}$). This indicates that the instantaneous loss rate of O_3 , $L(O_3)$, was large. Since the net change in concentration of any chemical species is the sum of its production and loss, i.e., $d[O_3]/dt = P(O_3) - L(O_3)$, $L(O_3)$ can be calculated from

$$L(O_3) = k'(O_3) \times [O_3] = P(O_3) - d[O_3]/dt \quad (10)$$

Here, $k'(O_3)$ is the pseudo-first order O_3 loss rate constant.

Figure 23 shows the time-of-day dependence of the pseudo-first order O_3 loss rate constant, color-coded by NO_x . The O_3 loss rate constant scales with NO_x , which indicates that the primary O_3 loss process at this site was by titration with freshly emitted NO via reaction (6). Conversion of NO_2 to NO_z , which removes O_x [Wood *et al.*, 2009], likely also contributed to O_3 loss.

At lower NO_x levels, a lower limit to O_3 loss is set by its dry deposition. Figure 23 shows first-order loss rate constant for O_3 with respect to dry deposition, calculated assuming a dry deposition velocity of $v_d = 1 \text{ cm s}^{-1}$ [Wesely and Hicks, 2000] and boundary layer heights (h_{BL}) of 100, 500 or 1500 m. Even if a very shallow BL height of 100 m is assumed, dry deposition alone does not rationalize the observed O_3 loss rate. Hence, another process also removes O_3 at this site, likely reactions of O_3 with biogenic alkenes. Unfortunately, relevant VOC data are not yet available at the time of this report.

Production of OH and Cl radicals

When the rate of O₃ production is VOC-limited, the production of O₃ is directly proportional to the production rate of HO_x radicals, i.e., the photochemical production rate of OH [*Jacob*, 1999], which can be calculated from

$$P(\text{OH}) = 2k_{11}[\text{O}^1\text{D}][\text{H}_2\text{O}] = \frac{2k_{11}j(\text{O}^1\text{D})}{k_{11}[\text{H}_2\text{O}] + k_q[\text{M}]}[\text{H}_2\text{O}][\text{O}_3] \quad (11)$$

where $k_q[\text{M}] = k_{q,1}[\text{O}_2] + k_{q,2}[\text{N}_2]$ is the rate constant for conversion of O(¹D) to O(³P). The photolysis of ClNO₂ produces Cl atoms at a rate of

$$P(\text{Cl}) = j(\text{ClNO}_2) [\text{ClNO}_2] \quad (12)$$

Figure 24 shows time series of P(OH) and P(Cl) for the campaign. Close-up of Aug 2 (the morning with the highest ClNO₂ concentration) and Aug 3 are shown in Figure 25. The time-of-day dependence is shown in Figure 26. P(OH) is usually much greater than P(Cl), except for the early morning hours. In spite of the fairly low ClNO₂ concentrations observed during this study, reaction (12) contributed to the radical production in the morning hours (median value of ~12% of the total at 8 am, 2.5 hours after sunrise). On the mornings of Aug 2 and 3, production of Cl exceeded that of OH. Overall, though, the contributions of Cl to the radical budgets and O₃ production were small.

Conclusions

The study was a success in that a comprehensive 2-week-long set of relevant data was acquired as had been proposed. However, only modest to low pollution levels were encountered, and conditions required leading to O₃ exceedences did not develop. Thus, the prime objective of this study, to determine the concentrations of N₂O₅ and ClNO₂ when there are episodes of poor air quality, could not be achieved, and the full potential impact of nocturnal ClNO₂ formation could not be assessed.

However, many things were learned about nocturnal nitrogen oxide chemistry at T45. Mixing ratios of N₂O₅ and ClNO₂ were much lower than had been anticipated because of considerable nocturnal O₃ titration events, rationalized by significant nocturnal stratification. In addition, the yields of ClNO₂ (with respect to the nocturnal production rate of NO₃) were small (<10%). In the absence of VOC data, it is not clear to what extent titration of NO₃ by monoterpenes and isoprene competed with ClNO₂ formation; however, because the equilibrium ratio of N₂O₅:NO₃ was large (as large as 60:1), it stands to reason that ClNO₂ formation can be competitive. The highest ClNO₂ mixing ratio observed was 116 pptv (2.6% of NO_y). Since most of NO_y was in the form of NO_x at this site, it can be concluded that the impact of ClNO₂ formation on the lifetime of NO_x and odd nitrogen budgets were negligible during the relatively clean conditions encountered in this campaign. The box model indicates that heterogeneous hydrolysis of N₂O₅ removed up to 0.5 ppbv of NO_x, which is small compared to what is removed during daytime, e.g., by reaction of OH with NO₂. Thus, it can also be concluded that N₂O₅ chemistry only had a minor impact on NO_x and NO_y budgets during this study.

Under the clean to modestly polluted conditions observed in this pilot study, the contribution of ClNO₂ photolysis to the overall radical budgets was small. The only exceptions were the mornings of Aug 2 and 3, when ClNO₂ photolysis contributed up to 100 pptv of Cl atoms. However, there is no evidence that this led to a significant enhancement in O₃ on those days.

There are strong indications in this data set (the regular increase in ClNO₂ concentration after sunrise when the nocturnal boundary layer breaks up) to show that the chemistry was occurring more efficiently in air masses aloft and decoupled from the surface. In addition, higher ClNO₂ concentrations were observed when the Hysplit back trajectories connected to the Juan de Fuca Strait (on Aug 1/2). This suggests that a follow-up study, either at an elevated location or closer to the coast (e.g., at Saturna Island [McLaren *et al.*, 2010]), and when the region is experiencing an episode of poor air quality, should be conducted to assess the impact of nocturnal nitrogen oxide chemistry in the LFV region. Because of the nocturnal stratification, T45 would not be the best location to observe this chemistry.

Table 1: Measurements conducted by the University of Calgary

Species	Method	Uncertainty	Max. time resolution	Current status
NO ₂	Blue diode laser cavity ring-down spectroscopy (custom instrument)	±10%	1 s	final
NO	O ₃ -Chemiluminescence (Thermo 42i-Y)	±30%	10 s	final
NO _y	O ₃ -Chemiluminescence and heated Mo converter (Thermo 42i-Y); operated with inlet filter	±30%	10 s	final
N ₂ O ₅	Red diode cavity ring-down spectroscopy (custom instrument)	±25%	1 s	final
PAN, PPN	Gas chromatography with electron capture detection (custom instrument)	±10%	6 min	final
O ₃	UV absorption (Thermo 49i)	±10%	10 s	final
j(NO ₂), j(NO ₃), j(O ¹ D), j(ClNO ₂)	Spectral radiometry (Metcon)	±20%	10 s	final
ClNO ₂	Chemical ionization mass spectrometry (custom instrument)	±25%	30 s	final
PAN, PPN, MPAN, etc.	Chemical ionization mass spectrometry (custom instrument)	±10%	30 s	not used

Table 2: Measurements conducted by Metro Vancouver

Species	Method	Uncertainty	Max. time resolution	Current status
Met data (temperature, wind speed + direction, relative humidity, precipitation, atmospheric pressure)	misc.	tbd	1 min	raw*
NO	O ₃ -Chemiluminescence (Thermo 17i)	tbd	1 min	raw*
NO ₂	O ₃ -Chemiluminescence and heated Mo converter (Thermo 17i)	tbd	1 min	raw*
NH ₃	O ₃ -Chemiluminescence and stainless steel converter (Thermo 17i)	tbd	1 min	raw*
O ₃	UV absorption	tbd	1 min	raw*
CO	Nondispersive infrared	tbd	1 min	raw*
SO ₂	UV Fluorescence	tbd	1 min	raw*
PM 10	Tempered Element Oscillating Microbalance (TEOM)	tbd	1 min	raw*
PM 2.5	TEOM	tbd	1 min	raw*

* Only "raw", not quality-assured data has so far been made available.

Table 3: Measurements conducted by Environment Canada

Species	Method	Uncertainty	Max. time resolution	Current status
Aerosol size distribution	Scanning mobility particle sizer (SMPS)	tbd	tbd	data reduction planned for 2013; data have not yet been shared with UC
Aerosol composition	Aerosol Chemical Speciation Monitor (ACSM)	tbd	tbd	
Isoprene and other VOCs	Gas chromatography - mass spectrometry	tbd	tbd	

Figure 1: Time series of NO, NO₂, and NO_y measured by the University of Calgary (UC).

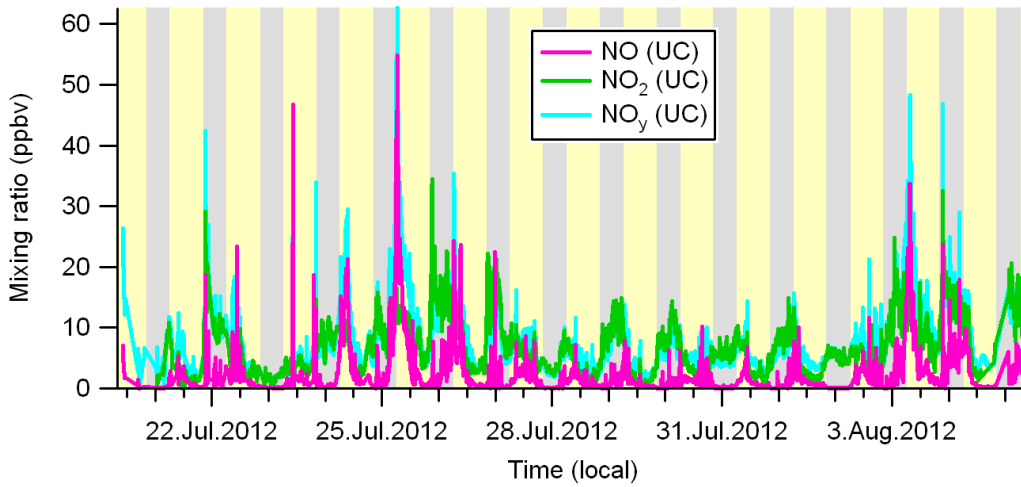


Figure 2: Time of day-dependence of NO_x (= NO + NO₂), NO, and NO₂. For each species, the median and 25% and 75% percentiles are displayed.

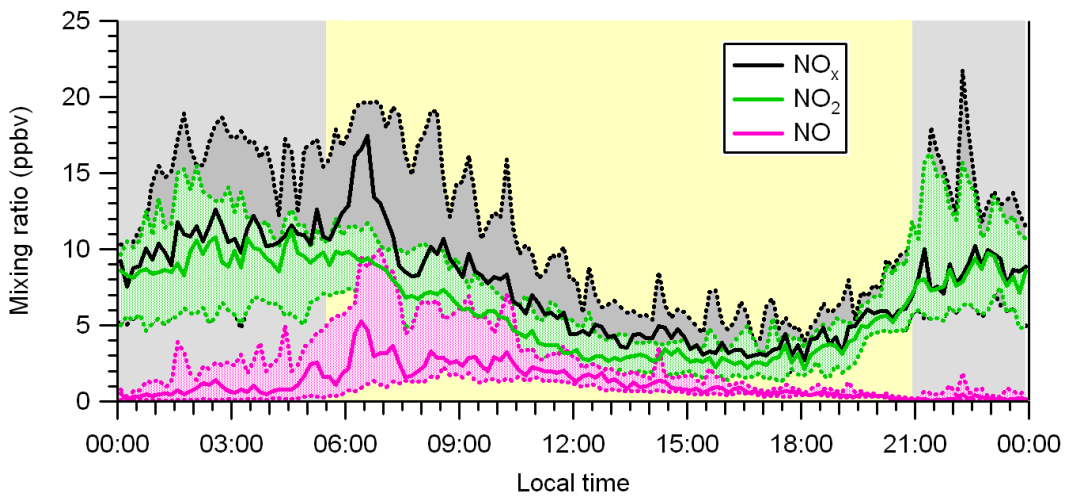


Figure 3: Time series of O₃ and odd oxygen (O_x = O₃ + NO₂) measured by the University of Calgary (UC).

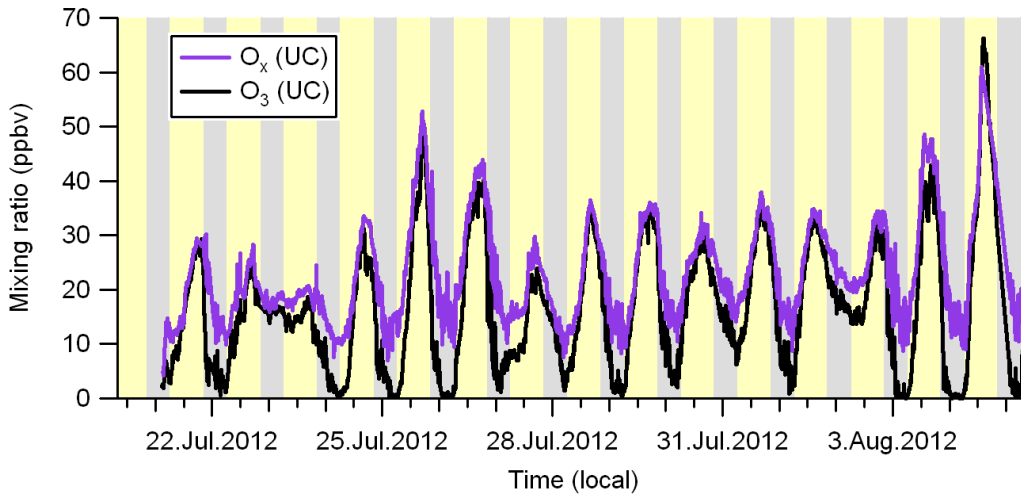


Figure 4: Time of day-dependence of NO_x (= NO + NO₂), O₃, and O_x. For each species, the median and 25% and 75% percentiles are displayed.

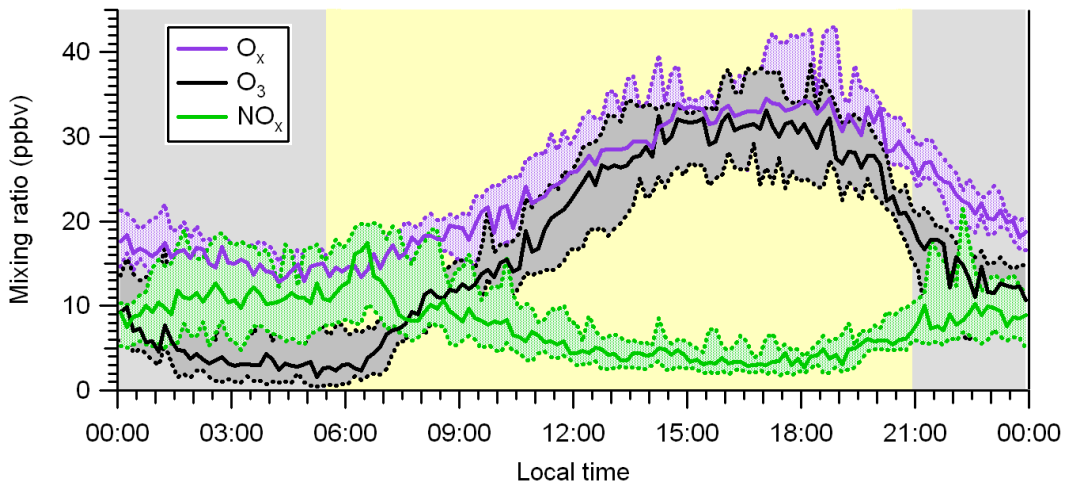


Figure 5: Mixing ratios of the nocturnal nitrogen oxides ClNO_2 and N_2O_5 .

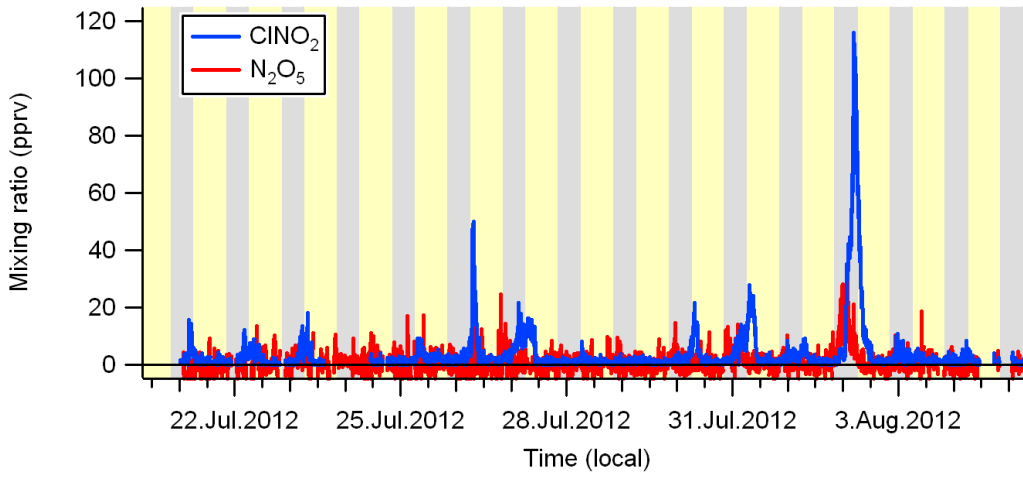


Figure 6. Time of day-dependence of ClNO_2 and N_2O_5 . For each species, the median and 25% and 75% percentiles are displayed.

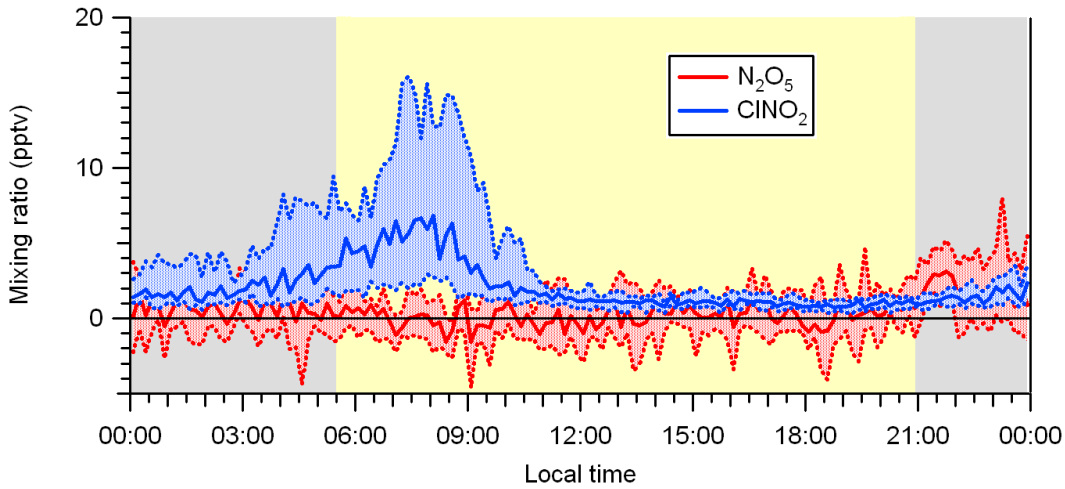


Figure 7. Mixing ratios of ClNO_2 and N_2O_5 on the night of Aug 1/2.

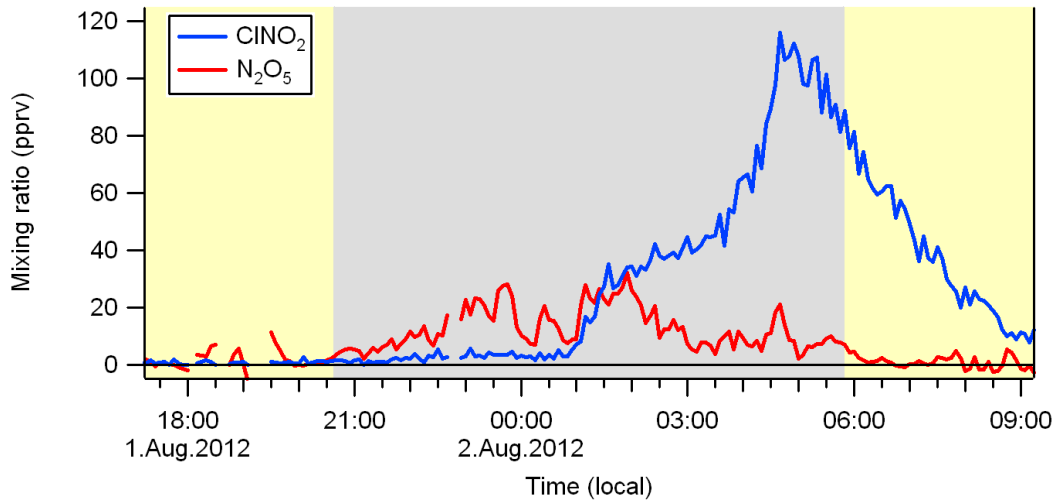


Figure 8. HYSPLIT back trajectory for the night of Aug 1/2.



Figure 9. Comparison of observed and modeled CINO₂ mixing ratios. Assumptions made in this model run: $\gamma(\text{N}_2\text{O}_5) = 0.025$, $S(\text{aerosol}) = 200 \mu\text{m}^2 \text{cm}^{-3}$, $\phi(\text{CINO}_2) = 10\%$.

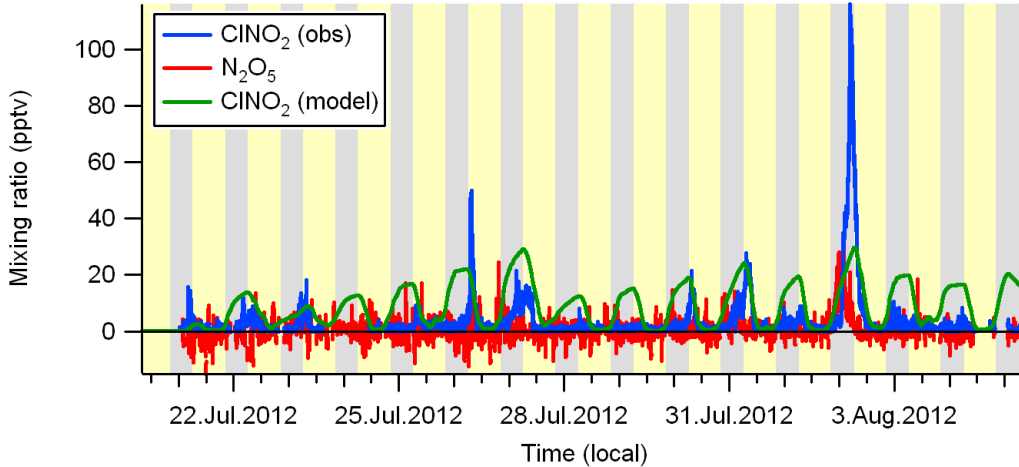


Figure 10. Comparison of observed and modeled CINO₂ mixing ratios for the night of Aug 1/2. Assumptions made in this model run: $\gamma(\text{N}_2\text{O}_5) = 0.025$, $S(\text{aerosol}) = 200 \mu\text{m}^2 \text{cm}^{-3}$, $\phi(\text{CINO}_2) = 30\%$.

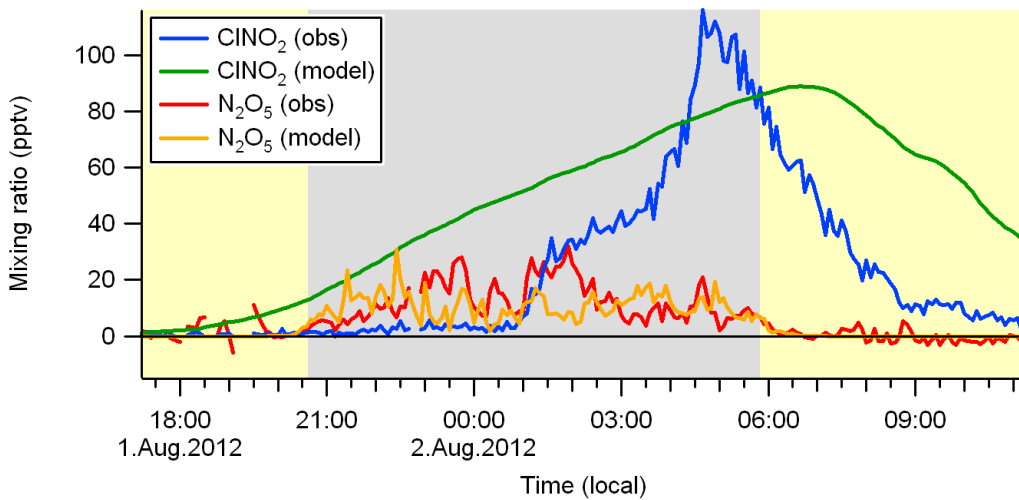


Figure 11: Time series of PAN and PPN mixing ratios.

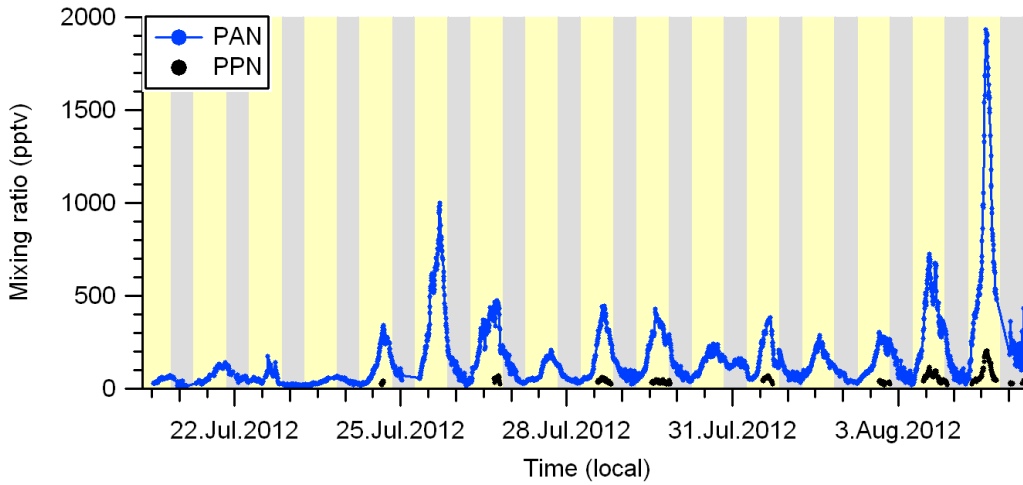


Figure 12: Time of day-dependence of PAN (median values shown). The median and 25% and 75% percentiles are also displayed. The median O_3 mixing ratio (multiplied by 0.01) is superimposed.

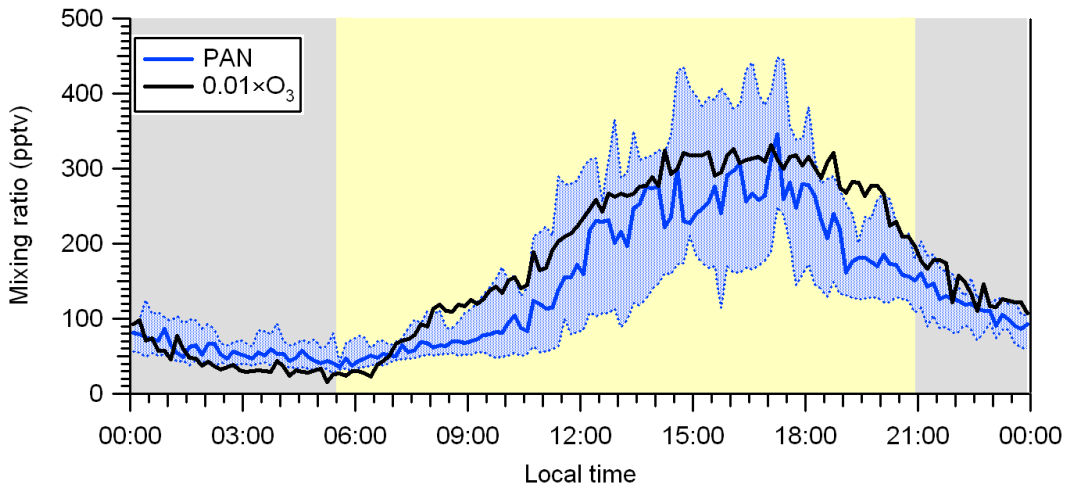


Figure 13: Scatter plots of PAN and PPN mixing ratios against those of O₃.

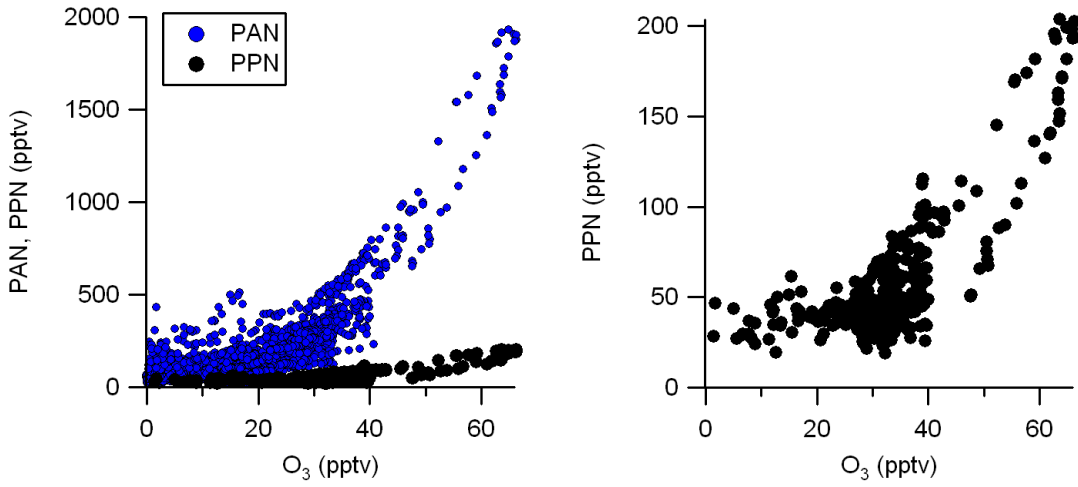


Figure 14: Time series of PAN and PPN mixing ratios relative to those of NO_y.

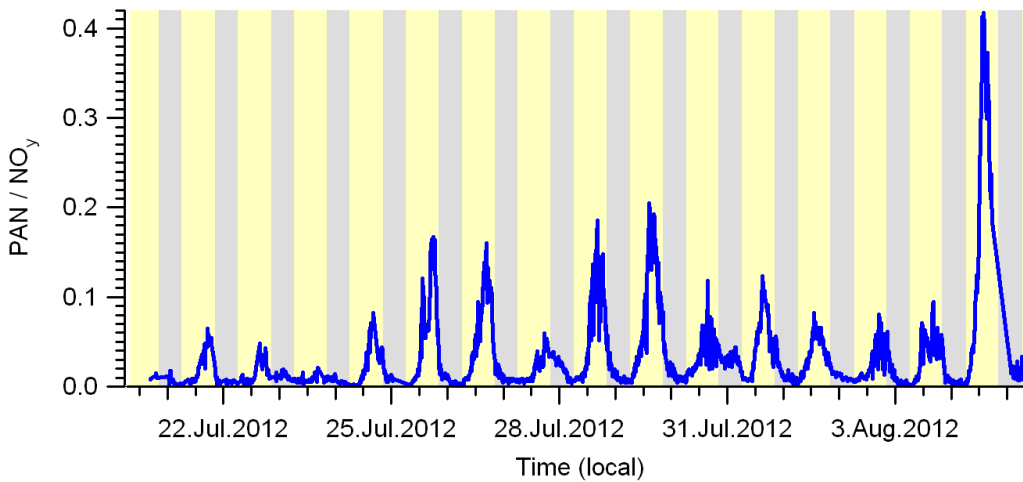


Figure 15: Scatter plot of PPN against PAN mixing ratios. The slope is sensitive to whether the O₃ production proceeds via oxidation of anthropogenic hydrocarbons (i.e., oxidation of propene and propanal) vs. oxidation of acetaldehyde, which is derived mainly from biogenic sources.

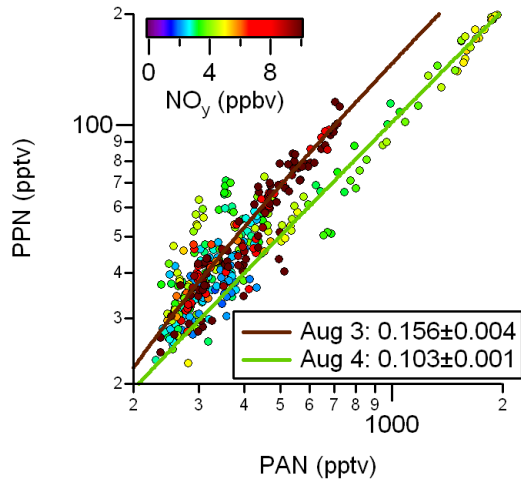


Figure 16: Time series of air temperature.

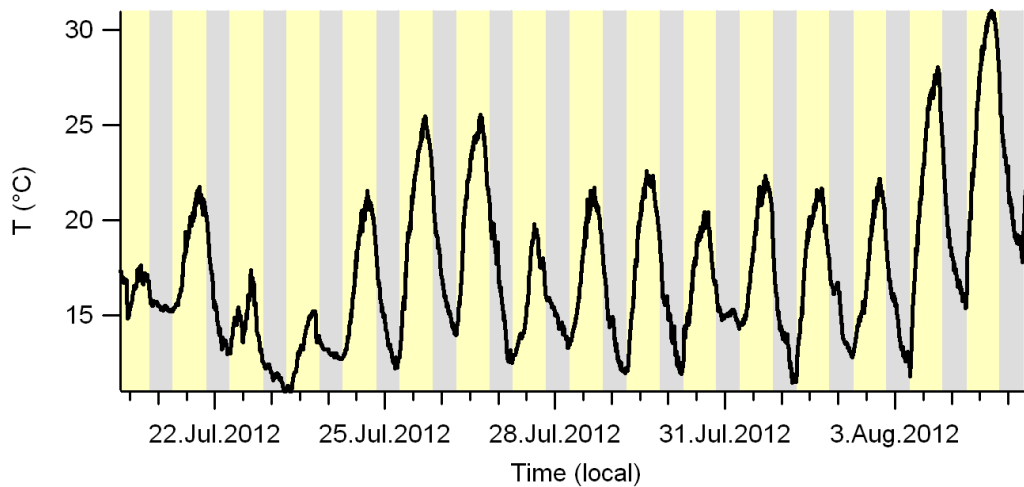


Figure 17: Time series of selected measured photolysis rate constants.

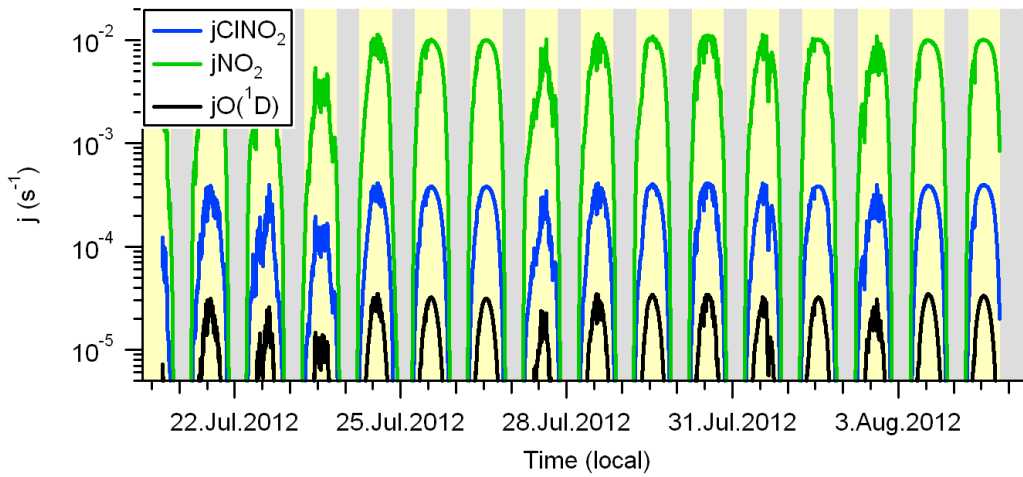


Figure 18: Comparison of observed photolysis rates with values predicted using NCAR's TUV model (http://cprm.acd.ucar.edu/Models/TUV/Interactive_TUV/) version 4.1 on a cloud-free day.

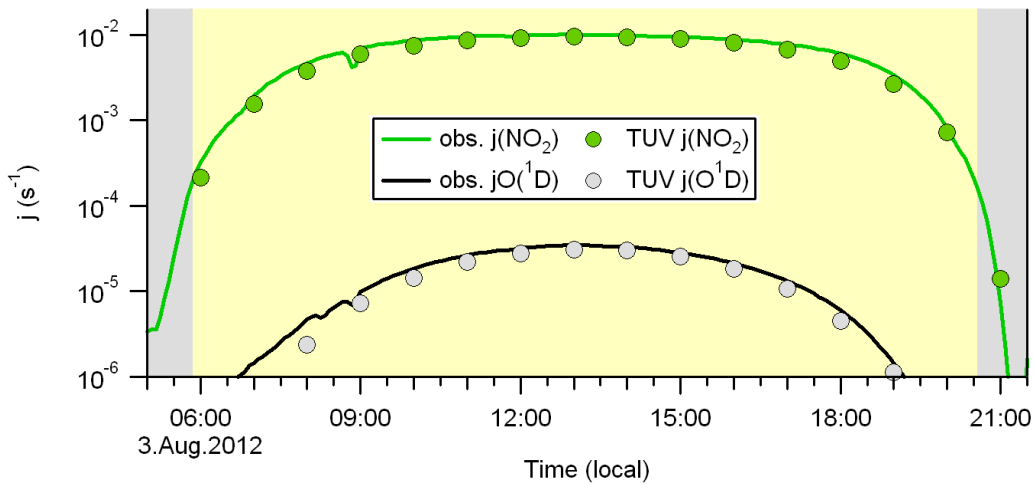


Figure 19: Time series of $P(O_3)$ calculated using equation (9).

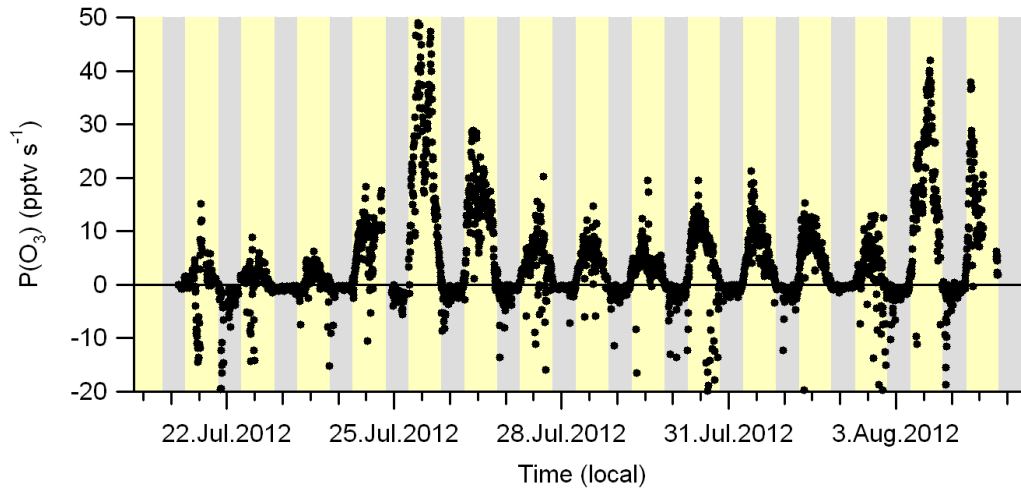


Figure 20: $P(O_3)$ calculated using equation (9) plotted against time of day and color-coded by temperature.

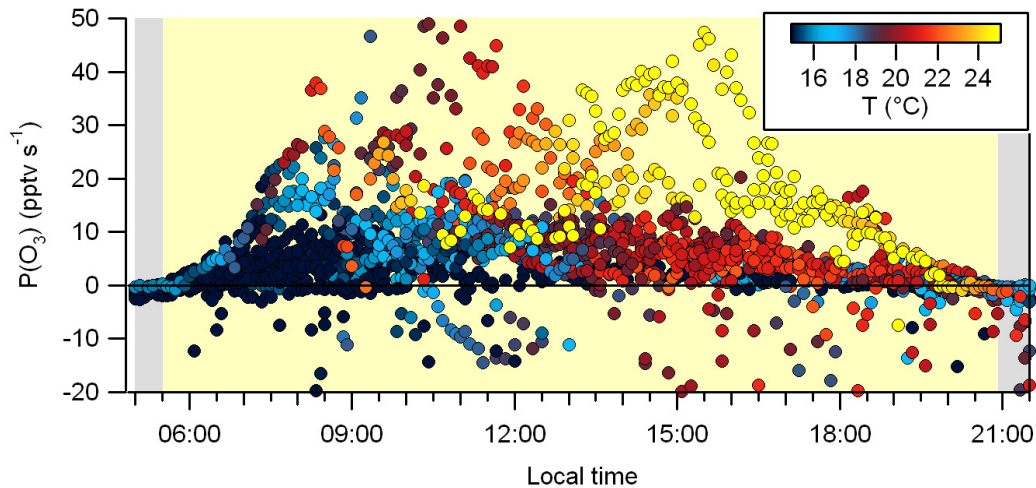


Figure 21: Time series of $d[O_3]/dt = P(O_3) - L(O_3)$, averaged over 30 min. The change in odd oxygen is superimposed.

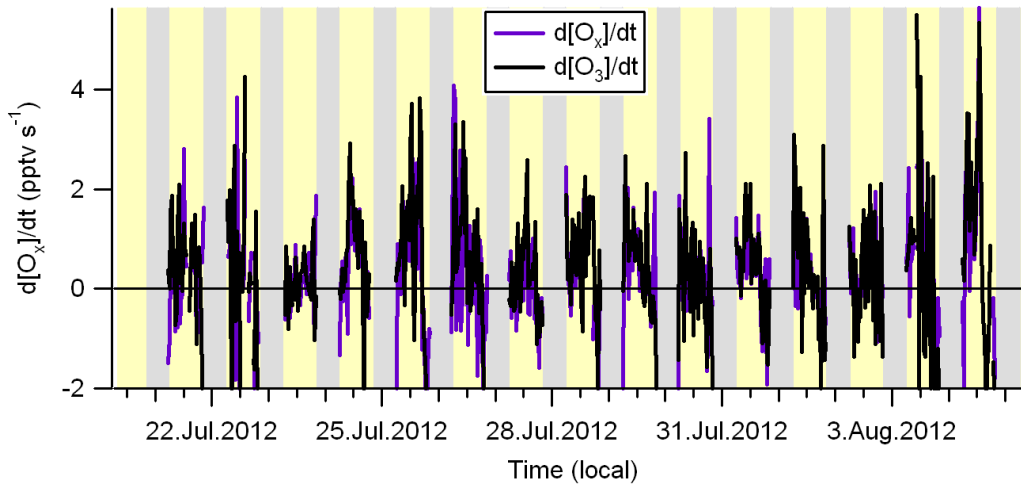


Figure 22: Time-of-day dependence of $d[O_3]/dt$ and $d[O_x]/dt$ averaged over 30 min.

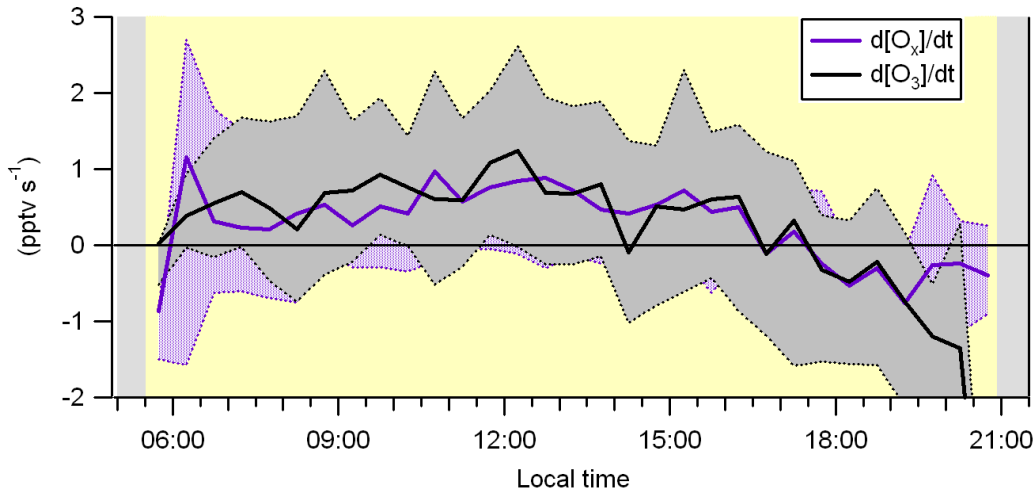


Figure 23: $k'(O_3)$ plotted against time of day and color-coded by NO_x . First-order loss rates due to dry deposition with 100 m, 500 m, or 1500 m mixing height and an assumed dry deposition velocity of 1 cm s^{-1} [Wesely and Hicks, 2000] are superimposed.

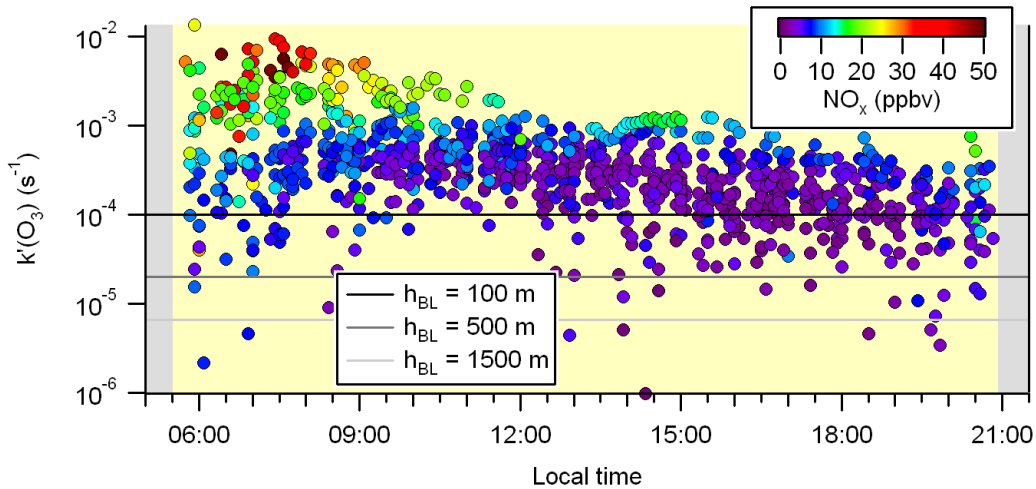


Figure 24: Radical production of OH (from $O^1D + H_2O$) and of Cl (from photolysis of $ClNO_2$).

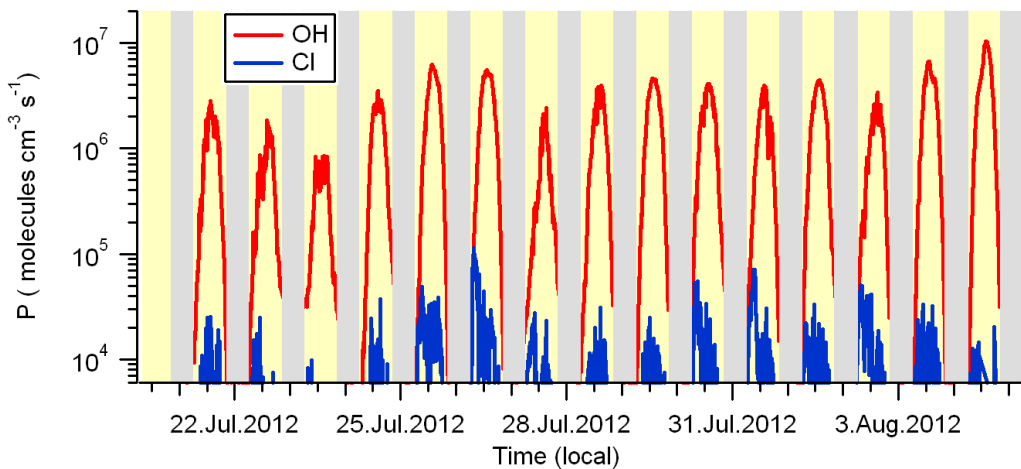


Figure 25: Radical production of OH (from $O^1D + H_2O$) and of Cl (from photolysis of $ClNO_2$) on the mornings of Aug 2 (top) and 3 (bottom).

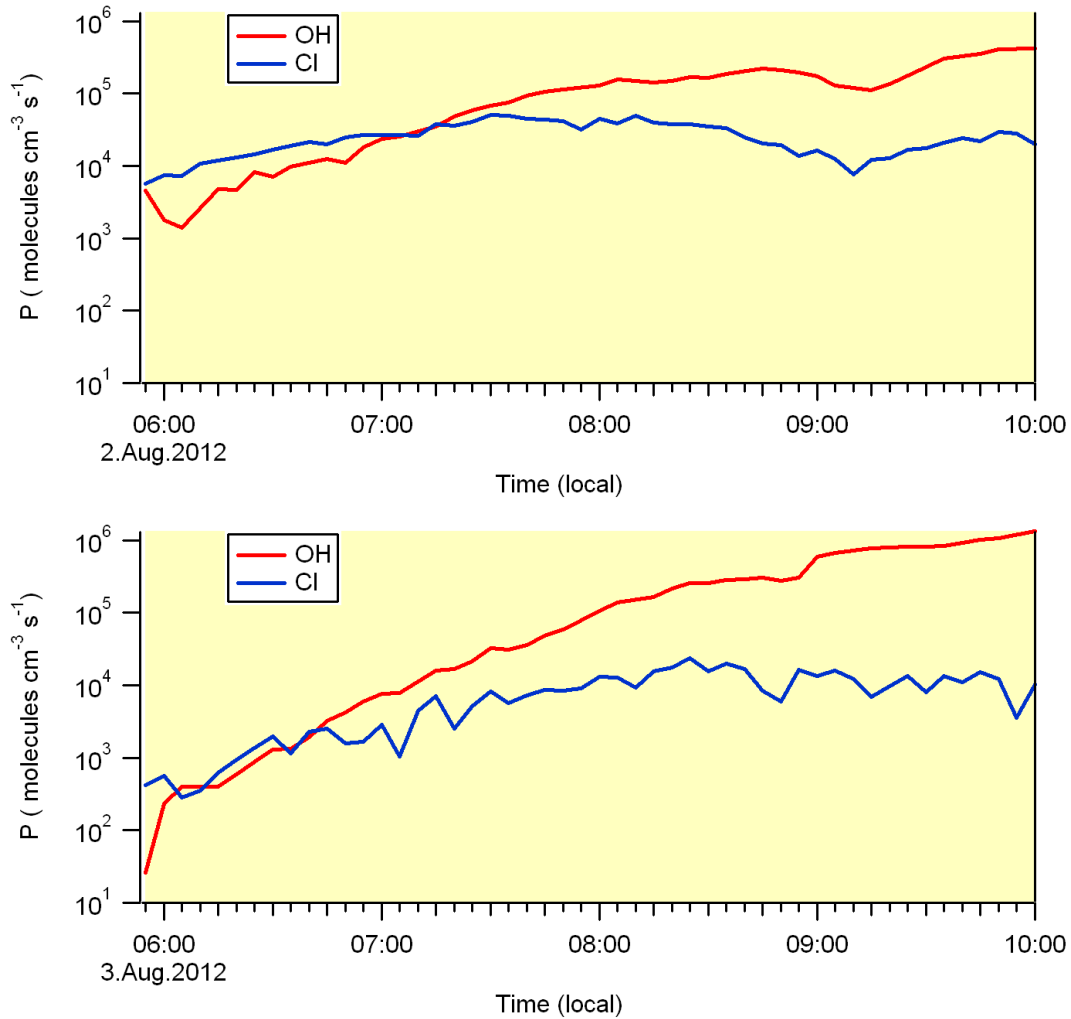
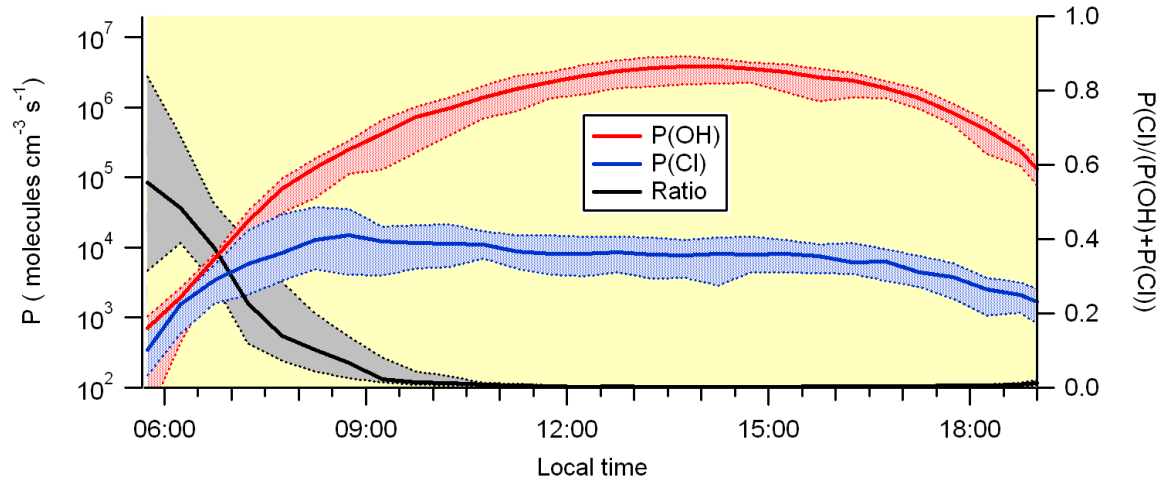


Figure 26: Comparison of radical production as a function of time of day. The shaded areas represent the 25th and 75th percentiles, and the solid line the median values.



References

- Alicke, B., A. Geyer, A. Hofzumahaus, F. Holland, S. Konrad, H. W. Patz, J. Schafer, J. Stutz, A. Volz-Thomas, and U. Platt (2003), OH formation by HONO photolysis during the BERLIOZ experiment, *J. Geophys. Res.*, *108*(D4), 8247, doi:8210.1029/2001JD000579.
- Anlauf, K., S.-M. Li, R. Leaitch, J. Brook, K. Hayden, D. Toom-Sauntry, and A. Wiebe (2006), Ionic composition and size characteristics of particles in the Lower Fraser Valley: Pacific 2001 field study, *Atmos. Environm.*, *40*(15), 2662-2675.
- Behnke, W., C. George, V. Scheer, and C. Zetzsch (1997), Production and decay of ClNO₂, from the reaction of gaseous N₂O₅ with NaCl solution: Bulk and aerosol experiments, *J. Geophys. Res.*, *102*(D3), 3795-3804, doi:10.1029/96JD03057
- Bertram, T. H., and J. A. Thornton (2009), Toward a general parameterization of N₂O₅ reactivity on aqueous particles: the competing effects of particle liquid water, nitrate and chloride, *Atmos. Chem. Phys. Discuss.*, *9*(4), 15181-15214.
- Finlayson-Pitts, B. J., M. J. Ezell, and J. N. Pitts (1989), Formation Of Chemically Active Chlorine Compounds By Reactions Of Atmospheric NaCl Particles With Gaseous N₂O₅ And ClONO₂, *Nature*, *337*(6204), 241-244, doi:10.1038/337241a0
- Ghosh, B., D. K. Papanastasiou, R. K. Talukdar, J. M. Roberts, and J. B. Burkholder (2011), Nitryl Chloride (ClNO₂): UV/Vis Absorption Spectrum between 210 and 296 K and O(³P) Quantum Yield at 193 and 248 nm, *J. Phys. Chem. A*, *116*(24), 5796-5805, doi:10.1021/jp207389y.
- Grosjean, E., D. Grosjean, M. P. Fraser, and G. R. Cass (1996), Air quality model evaluation data for organics .3. Peroxyacetyl nitrate and peroxypropionyl nitrate in Los Angeles air, *Environm. Sci. Technol.*, *30*(9), 2704-2714, doi:10.1021/es9508535.
- Hayden, K. L., K. G. Anlauf, S. M. Li, A. M. Macdonald, J. W. Bottenheim, J. R. Brook, and H. A. Wiebe (2004), Characterization of gaseous nitrogen oxides in the Lower Fraser Valley during Pacific 2001, *Atmos. Environm.*, *38*(34), 5811-5823.
- Hofzumahaus, A., A. Kraus, A. Kylling, and C. S. Zerefos (2002), Solar actinic radiation (280-420 nm) in the cloud-free troposphere between ground and 12 km altitude: Measurements and model results, *J. Geophys. Res.*, *107*(D18), 8139, doi:10.1029/2001JD900142.
- Hofzumahaus, A., A. Kraus, and M. Muller (1999), Solar actinic flux spectroradiometry: a technique for measuring photolysis frequencies in the atmosphere, *Applied Optics*, *38*(21), 4443-4460.
- Jacob, D. J. (1999), *Introduction to atmospheric chemistry*, xii, 266 p. pp., Princeton University Press, Princeton, N.J.
- Junkermann, W., et al. (2002), Actinic radiation and photolysis processes in the lower troposphere: Effect of clouds and aerosols, *Journal of Atmospheric Chemistry*, *42*(1), 413-441.
- Kercher, J. P., T. P. Riedel, and J. A. Thornton (2009), Chlorine activation by N₂O₅: simultaneous, in situ detection of ClNO₂ and N₂O₅ by chemical ionization mass spectrometry, *Atmos. Meas. Tech.*, *2*(1), 193-204, doi:10.5194/amt-2-193-2009.
- Knipping, E. M., and D. Dabdub (2003), Impact of chlorine emissions from sea-salt aerosol on coastal urban ozone, *Environm. Sci. Technol.*, *37*(2), 275-284, doi:10.1021/es025793z

- Koppmann, R. (2007), *Volatile organic compounds in the atmosphere*, 1st ed., Blackwell Pub., Oxford ; Ames, Iowa.
- Kraus, A., and A. Hofzumahaus (1998), Field measurements of atmospheric photolysis frequencies for O₃, NO₂, HCHO, CH₃CHO, H₂O₂, and HONO by UV spectroradiometry, *Journal of Atmospheric Chemistry*, 31(1-2), 161-180.
- Leighton, P. A. (1961), *Photochemistry of air pollution*, Academic Press, San Diego, CA.
- Malowicki, S. M. M., R. Martin, and M. C. Qian (2008), Volatile Composition in Raspberry Cultivars Grown in the Pacific Northwest Determined by Stir Bar Sorptive Extraction–Gas Chromatography–Mass Spectrometry, *Journal of Agricultural and Food Chemistry*, 56(11), 4128-4133, doi:10.1021/jf073489p.
- McLaren, R., R. A. Salmon, J. Liggiio, K. L. Hayden, K. G. Anlauf, and W. R. Leitch (2004), Nighttime chemistry at a rural site in the Lower Fraser Valley, *Atmos. Environm.*, 38(34), 5837-5848.
- McLaren, R., P. Wojtal, D. Majonis, J. McCourt, J. D. Halla, and J. Brook (2010), NO₃ radical measurements in a polluted marine environment: links to ozone formation, *Atmos. Chem. Phys.*, 10(9), 4187-4206, doi:10.5194/acp-10-4187-2010.
- Mielke, L. H., A. Furgeson, and H. D. Osthoff (2011), Observation of ClNO₂ in a mid-continental urban environment, *Environm. Sci. Technol.*, 45(20), 8889-8896, doi:10.1021/es201955u.
- Osthoff, H. D., et al. (2008), High levels of nitryl chloride in the polluted subtropical marine boundary layer, *Nature Geosci.*, 1(5), 324-328, doi:10.1038/ngeo177.
- Phillips, G. J., M. J. Tang, J. Thieser, B. Brickwedde, G. Schuster, B. Bohn, J. Lelieveld, and J. N. Crowley (2012), Significant concentrations of nitryl chloride observed in rural continental Europe associated with the influence of sea salt chloride and anthropogenic emissions, *Geophys. Res. Lett.*, 39(10), L10811, doi:10.1029/2012gl051912.
- Raff, J. D., B. Njagic, W. L. Chang, M. S. Gordon, D. Dabdub, R. B. Gerber, and B. J. Finlayson-Pitts (2009), Chlorine activation indoors and outdoors via surface-mediated reactions of nitrogen oxides with hydrogen chloride, *Proc. Natl. Acad. Sci. U. S. A.*, 106(33), 13647-13654, doi:10.1073/pnas.0904195106.
- Riedel, T. P., et al. (2012), Nitryl Chloride and Molecular Chlorine in the Coastal Marine Boundary Layer, *Environm. Sci. Technol.*, 46(19), 10463-10470, doi:10.1021/es204632r.
- Roberts, J. M. (2007), PAN and Related Compounds, in *Volatile Organic Compounds in the Atmosphere*, edited by R. Koppmann, pp. 221-268, Blackwell Publishing, Oxford, UK.
- Roberts, J. M., F. Flocke, C. A. Stroud, D. Hereid, E. Williams, F. Fehsenfeld, W. Brune, M. Martinez, and H. Harder (2002), Ground-based measurements of peroxy-carboxylic nitric anhydrides (PANs) during the 1999 Southern Oxidants Study Nashville Intensive, *J. Geophys. Res.*, 107(D21), doi:4554 10.1029/2001jd000947.
- Roberts, J. M., H. D. Osthoff, S. S. Brown, and A. R. Ravishankara (2008), N₂O₅ oxidizes chloride to Cl₂ in acidic atmospheric aerosol, *Science*, 321(5892), 1059, doi:10.1126/science.1158777.
- Roberts, J. M., H. D. Osthoff, S. S. Brown, A. R. Ravishankara, D. Coffman, P. K. Quinn, and T. S. Bates (2009), Laboratory Studies of Products of N₂O₅ Uptake on Cl⁻

- Containing Substrates, *Geophys. Res. Lett.*, 36(L20), L20808, doi:20810.21029/22009GL040448.
- Roberts, J. M., et al. (1998), Measurements of PAN, PPN, and MPAN made during the 1994 and 1995 Nashville Intensives of the Southern Oxidant Study: Implications for regional ozone production from biogenic hydrocarbons, *J. Geophys. Res.*, 103(D17), 22473-22490.
- Sander, S. P., et al. (2006), *Chemical Kinetics and Photochemical Data for Use in Atmospheric Studies, Evaluation Number 15*, NASA/JPL, Pasadena, CA.
- Stark, H., B. M. Lerner, R. Schmitt, R. Jakoubek, E. J. Williams, T. B. Ryerson, D. T. Sueper, D. D. Parrish, and F. C. Fehsenfeld (2007), Atmospheric in situ measurement of nitrate radical (NO₃) and other photolysis rates using spectroradiometry and filter radiometry, *J. Geophys. Res.*, 112(D10), D10S04, doi:10.1029/2006JD007578.
- Steyn, D. G., J. W. Bottenheim, and R. B. Thomson (1997), Overview of tropospheric ozone in the Lower Fraser Valley, and the Pacific '93 field study, *Atmos. Environm.*, 31(14), 2025-2035.
- Tanaka, P. L., et al. (2003), Direct evidence for chlorine-enhanced urban ozone formation in Houston, Texas, *Atmos. Environm.*, 37(9-10), 1393-1400, doi:10.1016/S1352-2310(02)01007-5
- Thornton, J. A., et al. (2002), Ozone production rates as a function of NO_x abundances and HO_x production rates in the Nashville urban plume, *J. Geophys. Res.*, 107(D12), 4146, doi:4110.1029/2001JD000932.
- Vingarzan, R., and S. M. Li (2006), The Pacific 2001 Air Quality Study - synthesis of findings and policy implications, *Atmos. Environm.*, 40(15), 2637-2649, doi:10.1016/j.atmosenv.2005.09.083.
- Wesely, M. L., and B. B. Hicks (2000), A review of the current status of knowledge on dry deposition, *Atmos. Environm.*, 34(12-14), 2261-2282.
- Wood, E. C., et al. (2009), A case study of ozone production, nitrogen oxides, and the radical budget in Mexico City, *Atmos. Chem. Phys.*, 9(7), 2499-2516.